

# Guess What Moves: Unsupervised Video and Image Segmentation by Anticipating Motion

Subhabrata Choudhury\*, Laurynas Karazija\*,  
Iro Laina, Andrea Vedaldi, Christian Rupprecht

Visual Geometry Group  
University of Oxford  
Oxford, UK

subha, laurynas, iro, chrisr, vedaldi@robots.ox.ac.uk

## Abstract

Motion, measured via optical flow, provides a powerful cue to discover and learn objects in images and videos. However, compared to using appearance, it has some blind spots, such as the fact that objects become invisible if they do not move. In this work, we propose an approach that combines the strengths of motion-based and appearance-based segmentation. We propose to supervise an image segmentation network, tasking it with predicting regions that are likely to contain simple motion patterns, and thus likely to correspond to objects. We apply this network in two modes. In the unsupervised video segmentation mode, the network is trained on a collection of unlabelled videos, using the learning process itself as an algorithm to segment these videos. In the unsupervised image segmentation model, the network is learned using videos and applied to segment independent still images. With this, we obtain strong empirical results in unsupervised video and image segmentation, significantly outperforming the state of the art on benchmarks such as DAVIS, sometimes with a 5% IoU gap.

## 1 Introduction

The motion of objects in a video can be detected by methods such as optical flow and used to discover, segment and learn the objects. A key benefit is that optical flow is object-agnostic: because it relies on low-level visual properties, it can extract a signal even before the objects are learned, and can thus be used to *bootstrap* an understanding of objectness without manual supervision.

The potential of motion as a cue is probably best epitomised by the problem of *video segmentation*, where the input is a generic video sequence and the task is to extract the main object or objects in the video. Many video segmentation methods do not assume that a *a specific object or type of objects* is observed; instead, they leverage motion to discover the objects without assuming much prior information about them. In fact, recent state-of-the-art (SoTA) video segmentation methods, such as [53, 80], have taken the extreme view of *only* using optical flow, and hence motion, for segmentation, otherwise disregarding the appearance of the objects and arguing that motion patterns are much easier to model and interpret than appearance patterns.

In this paper, we moderate this view and re-emphasize the importance and usefulness of making the motion and appearance modality *collaborate* in learning and segmenting visual objects, particularly in the unsupervised case. We do so by learning an image-based segmentation network, and use optical-flow self-supervision to train it without manual supervision, tasking the network with antic-

---

\* Authors contributed equally.

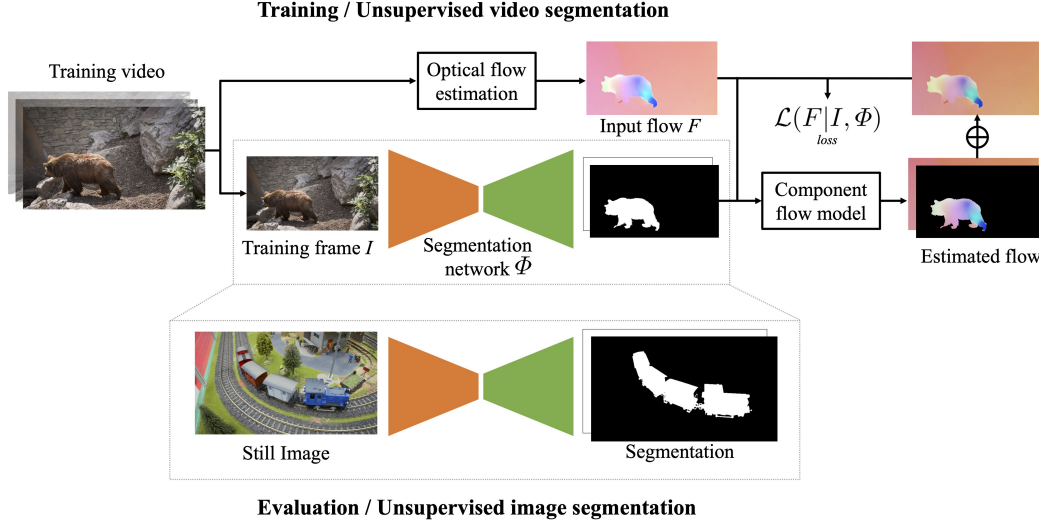


Figure 1: **Model Diagram.** Network is trained using videos with loss formulated as error between estimated optical flow using component flow model and input flow (4). The network can then perform inference using only still images

ipating the optical flow given a single image as input. Because motion *cannot* usually be predicted unambiguously from a single image, the network is asked to predict regions where the optical flow vectors are *likely to be arranged according to particularly simple patterns*—for example, constant or affine. The idea is that such regions, exhibiting coherent flow patterns within, roughly correspond to independent objects.

Compared to using only optical flow for segmenting objects, using appearance too has a few clear advantages. The most obvious one is that, while objects do move *occasionally*, they do not necessarily move *all the time*. On the other hand, appearance always provides a cue about the presence of objects,<sup>1</sup> providing complementary evidence for them, particularly when motion is lacking. Furthermore, appearance patterns are usually more distinctive than motion patterns and better allow to identify and distinguish different objects. As an added bonus, because the network operates on the appearance modality, any number of pre-training techniques, unsupervised and supervised, can be used to pre-train the segmentation network, boosting performance.

For image segmentation, we use a collection of videos for training the network and test it on an independent test set of still images. For video segmentation, however, the network cannot by itself exploit motion information because it operates on individual frames. A simple way of extending the method to use motion cues for inference is given by the video segmentation protocol of [80, 82]. Here, the unsupervised learning process itself is used as a segmentation algorithm: it receives as input the videos (and their pre-computed optical flow) and outputs their segmentation. The difference is that, while our network takes a single still image as input, it is also influenced by the corresponding optical flow via back-propagation.<sup>2</sup>

Our model achieves a significant boost in unsupervised video segmentation on three benchmark datasets, sometimes with a large 5% IoU gap over the SoTA, thus proving that appearance provides powerful complementary cues even in the video segmentation task. Moreover, we demonstrate the strong generalization of our model on common unsupervised image segmentation benchmarks and even obtain SoTA performance on two out of four datasets.

<sup>1</sup>With the possible exception of camouflage [42].

<sup>2</sup>This is a form of “internal learning”, similar to the deep prior [71], or fitting an appearance or deformation network to a single image collection as in [36, 54].

## 2 Related Work

Our work aims to combine motion and appearance cues for unsupervised object discovery, in that motion can be used as a cue to learn a general object segmenter for both videos and still images alike. As such, there is a connection to several related areas in literature, which we review next.

**Unsupervised Video Object Segmentation.** The aim of video object segmentation (VOS) is to densely label objects present in a video. Current VOS benchmarks [43, 57, 60] usually define the problem as foreground-background separation where the most salient objects in the scene typically form the foreground. Recently, there have been efforts to reduce the amount of supervision and two main directions that have gained significant attention are semi-supervised and unsupervised VOS. At test time, semi-supervised VOS requires manual annotations for the objects of interest for an initial frame and the goal is to re-localize (segment) them across the video [10]. Unsupervised VOS aims to discover the object(s) of interest without having the initial targets provided [22, 26, 44, 50, 59, 68]. However, despite what the name suggests, most unsupervised VOS methods in fact use some form of supervised pre-training on external data.

**Motion Segmentation.** In videos, the background is usually relatively static whereas objects in the scene have autonomous motion, thus providing a strong ‘objectness’ signal. Many works approach unsupervised video object segmentation as a motion segmentation problem. Brox et al. [8] leverage a point trajectory technique (e.g., [66]) to base segmentation on the long-term motion of tracked points. Several methods build on this idea and propose a multi-cut approach [37, 38, 39]. NLC [22] analyzes dominant motion in the optical flow to find the salient object, and uses appearance-based saliency as a fallback. FTS [59] generates object candidates from motion cues and refines them using appearance features. CIS [82] proposes an adversarial framework where an inpainter is tasked with guessing the optical flow of a segment based on contextual information, while the generator’s task is to create segments with zero mutual information to make the problem as difficult as possible for the inpainter. Layered models [11, 32] jointly optimize video segmentation and motion estimation. They are disadvantaged by their complicated and computationally expensive inference procedure. There have been efforts to find efficient approaches [70]. AMD [47] takes a different approach and uses separate pathways to segment the video frames and to model the motion, which makes inference simple. MG [80], in contrast, abandons appearance pathway altogether segmenting optical flow via scaled dot-product attention mechanism.

Another set of methods use optical flow to provide segmentations by merging pixels that are consistent with various motion models. Our method follows the same approach. [27] is one of the earliest works that attempts to model flow as a combination of smoothly varying layers. A set of work [4, 5] segments object translation directions from motion angle field obtained by correcting for estimated rotation of the camera. [69] instead considers a variety of probabilistic motion models selecting appropriate one by a version of Akaike information criterion. Similar to us, [51] considers affine flow model, however, uses entropy of flow magnitude histograms for loss to deal with noisy flow in real world. [53] consider affine and quadratic motion models, however their method uses flows as input which makes it suitable only for videos during inference.

**Unsupervised Image Segmentation.** In this work we consider the problem of binary segmentation of an image into foreground and background. The earlier works use hand-crafted priors, e.g., color contrast [14, 76], which do not perform as well as recent deep learning based methods. Deep learning based methods [56, 85, 86] typically combine multiple handcrafted heuristics to generate ground truth data and distill it using a deep network. [28, 58] proposed approaches based on mutual information maximization between different views of the input. A recently emerging line of work [2, 6, 12, 34, 52, 72] explores generative models to obtain segmentation masks. Many of them [2, 6, 12, 34] are based on the idea of generating foreground and background as separate layers and combine them to obtain a real image. Others [52, 72] analyze large-scale unsupervised GANs (e.g., BigGAN [7]) and find implicit foreground-background structure in them to generate a synthetic annotated training dataset. We show that our method can be used for this task, as it only requires a single image as input at test time, providing an alternative approach to unsupervised object segmentation that performs favorably in comparison to state-of-the-art methods.

**Unsupervised Object Discovery.** Different from previous methods that aim to segment the most salient object(s) in an image, unsupervised multi-object scene decomposition explores the prob-

lem of decomposing a scene into parts, which typically include each individual foreground object and the background. The usual approach is to learn structured object-centric representations, *i.e.* to model the scene with latent variables (slots) operating on a common representation [9, 15, 18, 20, 21, 24, 29, 45, 49]. While these methods are image-based, extensions to video also exist [1, 3, 16, 30, 33, 40, 41, 55, 84]. These methods often operate in an auto-encoding fashion with inductive bias to separate and segment objects derived from a reconstruction bottleneck [9]. This bottleneck of often learned reconstruction is architecture and latent-variable-model dependant [19], making it difficult to tune and complicating application. We similarly impose a reconstruction bottleneck on the flow. However, for ‘reconstruction’, we use a simple model grounded in projective geometry with a known closed form solution, which avoids such pitfalls. It is important to note that the unsupervised multi-object segmentation setting appears to be significantly more challenging, with current methods relying on synthetic scenes (e.g., CLEVR [31] for images or CATER [23] for videos) for their performance, while struggling on more realistic data [35].

### 3 Method

We learn to segment objects in an image by predicting which image regions are likely to move in a simple and distinctive manner. We supervise the model by matching its predictions to the optical flow obtained from video sequences.

Formally, let  $I \in \mathbb{R}^{3 \times H \times W} = (\mathbb{R}^3)^\Omega$  be an RGB image defined on a lattice  $\Omega = \{1, \dots, H\} \times \{1, \dots, W\}$ . For learning, the image is a frame in a video sequence and we denote with  $F \in (\mathbb{R}^2)^\Omega$  the corresponding optical flow image (which we compute from the video using an off-the-shelf optical flow network such as RAFT [67]). Our goal is to decompose the image into a foreground and a background region by learning to predict a binary mask  $m \in \{0, 1\}^\Omega$ . This can be achieved by learning a segmentation network  $\Phi(I) \in [0, 1]^\Omega$  that, given the image as input, assigns pixels  $u$  to foreground or background in a soft manner, with probabilities:

$$P(m_u = 1 | I, \Phi) = [\Phi(I)]_u, \quad m_u \in \{0, 1\}, \quad u \in \Omega. \quad (1)$$

In absence of ground truth mask annotations, one can exploit motion as a cue for learning. We can separate images into meaningful regions according to the motion within each region (principle of common fate [64, 73]). Specifically, each region  $m$  is associated with a model  $\theta_m$  of the optical flow pattern observed within it. We consider in particular *affine models*  $F_u \approx Au + b$  of the flow [51, 53], where  $\theta_m = (A_m, b_m)$  consists of a matrix  $A_m \in \mathbb{R}^{2 \times 2}$  and a vector  $b_m \in \mathbb{R}^2$ , and  $u \in \Omega$  are the coordinates of a pixel. We assume that the model predicts the flow up to Gaussian noise model with fixed isotropic standard deviation, which results in the simple  $L^2$  fitting loss:

$$-\log p(F_u | \theta_m) \propto \|F_u - A_m u - b_m\|^2. \quad (2)$$

Given the flow  $F$ , we minimize the energy function:

$$\begin{aligned} \mathcal{L}(F | \theta, I, \Phi) &= - \sum_{u \in \Omega} \sum_{m \in \{0, 1\}} \log p(F_u | \theta_m) \cdot p(m | I, \Phi) \\ &\propto \sum_{u \in \Omega} \sum_{m \in \{0, 1\}} \|F_u - A_m u - b_m\|^2 \cdot p(m_u | I, \Phi) \end{aligned} \quad (3)$$

Note that, in the expression above, we *do not* know the flow parameters  $\theta$  as the network only predicts the regions’ extent, not the actual flow pattern. Instead, we *min-out* the parameters in the loss, fitting the flow models  $\theta$

$$\mathcal{L}(F | I, \Phi) = \min_{\theta} \mathcal{L}(F | \theta, I, \Phi). \quad (4)$$

The energy in Eq. (2) is quadratic, resulting in a weighted least squares problem that can be efficiently solved in closed form (see supplementary material).

Intuitively, as the model takes as input only a single image, its task is to decompose the scene into regions that can generate the best possible fit for the flow model (Eq. (2)) without knowing the flow in advance. Therefore, the network is *not* tasked to predict the flow directly, which depends on the specific motion observed in the video and is ambiguous to infer from a single input image. As generally objects move independently of the background, and thus exhibit different flow patterns, our energy function effectively encourages the segmentation of objects through flow prediction.

**Compactness.** Foreground and background regions have so far been treated symmetrically. In order to distinguish them, we further regularize the foreground region  $m = 1$  to be spatially compact. We measure compactness as the average squared  $L^2$  distance between pixels in the foreground region:

$$\mathcal{L}_{\text{cmp}}(\Phi, I) = \sum_{u,v \in \Omega} \|u - v\|^2 \cdot P(m_u = 1 | \Phi, I) \cdot P(m_v = 1 | \Phi, I). \quad (5)$$

While a naive evaluation of this loss has cost  $O(|\Omega|^2)$ , in the sup. mat. we show how to compute it in cost  $O(|\Omega|)$  only.

**Training Formulation.** Our model is learned from a large collection  $\mathcal{T}$  of video frames-optical flow pairs  $(I, F)$ , minimizing the empirical risk:

$$\Phi^* = \underset{\Phi}{\operatorname{argmin}} \frac{1}{|\mathcal{T}|} \sum_{(I,F) \in \mathcal{T}} \lambda_a \mathcal{L}(F | I, \Phi) + \lambda_c \mathcal{L}_{\text{cmp}}(I, \Phi), \quad (6)$$

where  $\{\lambda_a, \lambda_c\} \in \mathbb{R}$  balances the influence of the two losses.

### 3.1 Justification and Model Improvements

The model above assumes that the observed optical flow  $F$  can be modelled in a piecewise-affine fashion:  $F_u \approx Au + b$ . If objects simply translate (maintaining their distance from the camera), the generated 2D flow is in fact affine (constant, with  $A = 0$ ) in the region. The same is true if the object rotates in-plane (in which case  $A \neq 0$ ) and, approximately, if the rotation is out-of-plane and the object is a small planar patch. However, other motions can result in more complex flow patterns that are not captured accurately by the simple affine model.

Rather than making the model more complex, we retain the affine approximation and pre-process the flow in a non-linear manner. The pre-processing has the added benefit of reducing the effect of outliers generated by the optical flow predictor. Specifically, we consider the non-linear mapping that compresses the magnitude of the flow vectors. If  $G \in (\mathbb{R}^2)^\Omega$  is the unprocessed 2D flow field, we use the normalized flow field:

$$F_u = \operatorname{clamp}_{[-\tau, \tau]^2} \frac{G_u}{\max_{v \in \Omega} |G_v|} \quad (7)$$

### 3.2 Two Modes: Video vs Image Segmentation

We experiment with two modes of application of our model. The first mode is *unsupervised video segmentation*. As the model operates on single images and not videos, we utilize the **process** of training the network (not just the resulting network itself) as a means of segmenting moving objects. We do not distinguish between training and testing; rather, the training process takes as input one or more unlabelled videos and their pre-computed optical flow and outputs the video segmentation. The network, which is learned as a byproduct, still only takes single images as input, but the training process utilizes optical flow information from the entire video. We can think of the network as a means for learning appearance and use it to regularize the motion segmentation, which is achieved by the network training process as a whole.

The second mode of operation is *image segmentation* mode. Here, the network is first trained using a number of unlabelled videos, and then applied to the task of single-image foreground object segmentation on an *independent* validation or test set of still images. In this mode, therefore, motion is only used as a supervisory signal: when the network is applied at test time, motion is not considered anymore and the network operates purely as an image-based segmenter. This can also be seen as an instance of *cross-modal self-supervision*.

## 4 Experiments

Our formulation allows us to evaluate our method in two settings: video segmentation and general image/object segmentation. We show that learning a network that *guesses what moves* not only results in state-of-the-art performance in video segmentation, but also generalizes to image segmentation without further training. Additionally, we experiment with different flow models  $\theta$  (Section 4.3), pre-training (Section 4.3), and unsupervised optical flow estimators (Section 4.3).

Table 1: **Unsupervised video segmentation** on DAVIS2016, SegTrack-v2 (STv2), and FBMS59, averaged over 5 random seeds ( $\pm\sigma$ ).  $\dagger$  denotes the usage of CRFs and other extra significant post-processing (e.g., multi-step flow, multi-crop, temporal smoothing for CIS [82]). Our network does not rely on optical flow for prediction, as illustrated in Table 6 for image segmentation

|                                  |                | Input |      | DAVIS16                        | STv2                           | FBMS59                         |
|----------------------------------|----------------|-------|------|--------------------------------|--------------------------------|--------------------------------|
|                                  |                | RGB   | Flow | $\mathcal{J} \uparrow$         | $\mathcal{J} \uparrow$         | $\mathcal{J} \uparrow$         |
| [75]                             | SAGE           | ✓     | ✓    | 42.6                           | 57.6                           | 61.2                           |
| [22]                             | NLC            | ✓     | ✓    | 55.1                           | 67.2                           | 51.5                           |
| [38]                             | CUT            | ✓     | ✓    | 55.2                           | 54.3                           | 57.2                           |
| [59]                             | FTS            | ✓     | ✓    | 55.8                           | 47.8                           | 47.7                           |
| [82]                             | CIS            | ✓     | ✓    | 59.2                           | 45.6                           | 36.8                           |
| [80]                             | MG             | ✗     | ✓    | 68.3                           | 58.6                           | 53.1                           |
| [53]                             | EM             | ✗     | ✓    | 69.8                           | –                              | –                              |
| <b>Ours</b> (UNet)               |                | ✓     | ✗    | 71.2 $\pm$ 0.5                 | 66.7 $\pm$ 1.5                 | 60.9 $\pm$ 0.6                 |
| <b>Ours</b> (MaskFormer)         |                | ✓     | ✗    | <b>71.2<math>\pm</math>0.2</b> | <b>69.0<math>\pm</math>0.8</b> | <b>66.9<math>\pm</math>0.2</b> |
| [82]                             | CIS $^\dagger$ | ✓     | ✓    | 71.5                           | 62.0                           | 63.5                           |
| <b>Ours<math>^\dagger</math></b> |                | ✓     | ✗    | <b>73.4<math>\pm</math>0.1</b> | <b>72.0<math>\pm</math>0.9</b> | <b>68.6<math>\pm</math>0.4</b> |

#### 4.1 Experimental Setup

**Architecture.** Our formulation enables us to use any standard image segmentation architecture for the model  $\Phi$ . This has two main benefits: while training the model needs optical flow (and thus video data), inference however can be performed on single images alone just like any image segmentation method. Second, using a standard architecture allows us to benefit from (self-)supervised pretraining ensuring better convergence and broader generalization (see Section 4.3). We experiment with both convolutional and transformer-based architectures, which we discuss later.

**Datasets.** For the *video segmentation* task, we use three popular datasets: DAVIS2016 (DAVIS16) [60], SegTrackV2 (STv2) [43], as well as FBMS59 [57]. DAVIS16 contains 30 training and 20 validation sequences with 3455 frames annotated at 480p resolution for the predominantly moving object. STv2 contains 14 sequences and 976 annotated frames, while FBMS59 has 59 sequences where every 20th frame is annotated (total 720 annotated frames). For the *image segmentation* task, we consider the Caltech-UCSD Birds-200 (CUB) dataset [77] and three saliency detection benchmarks: DUTS [74], ECSSD [63], and DUT-OMRON [81].

**Metrics.** We use the Jaccard index ( $\mathcal{J}$ ) to evaluate unsupervised video segmentation, calculated on pixels, taking the mean over the test set. Following the standard practice [26, 82], we combine multiple foreground objects in FBMS59 and STv2 datasets for comparison with other methods. Evaluation is performed in the original input resolution. For the unsupervised object segmentation task, we report pixel accuracy and the Jaccard index.

**Optical Flow.** As discussed in Section 3, our method derives learning signal from optical flow. We estimate optical flow for all frames on DAVIS16, STv2, and FBMS59 following the practice of MotionGrouping [80]. Namely, we employ three different approaches, RAFT [67] (supervised), PWC-Net [65] (supervised), and ARFlow [46] (unsupervised), using the original resolution, and gaps between frames of  $\{-2, -1, 1, 2\}$  for DAVIS16 and STv2, and  $\{-6, -3, 3, 6\}$  on FBMS59. RAFT is supervised on synthetic FlyingChairs [17] dataset.

**Training Details.** We use MaskFormer [13] as our segmentation network, and use only the segmentation head which is equivalent to their PerPixelBaseline+ model. For the backbone, we leverage the Swin-tiny transformer [48], pre-trained on ImageNet [62] in a self-supervised manner [78] to avoid external sources of supervision. The network is trained using AdamW optimiser, with learning rate of  $1.5 \times 10^{-4}$  and gradient clipping when 2-norm exceeds 0.01. We use batch size of 8 for 5k iterations only. We set  $\lambda_a=3e-2$ ,  $\lambda_c=1e-4$ ,  $\tau=0.33$  (6). The input RGB images and optical flows for loss assessment are interpolated to  $128 \times 224$  resolution using bi-cubic and nearest neighbor interpolation, respectively. Output segmentation logits are up-sampled using bi-linear interpolation to input resolution for training and again to annotation resolution for evaluation.



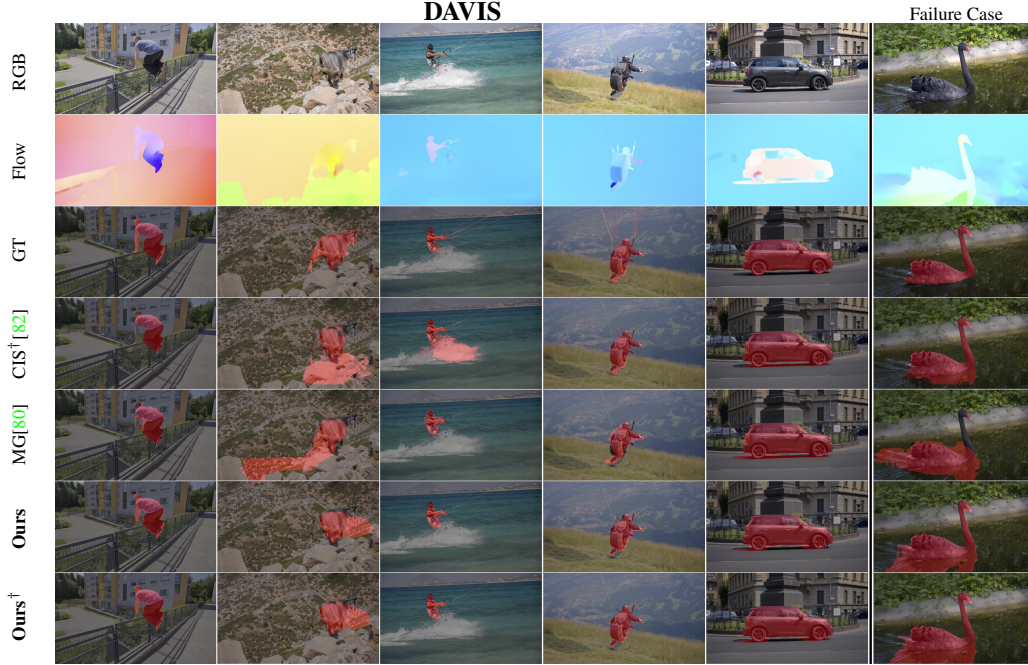


Figure 2: **Qualitative Comparison on DAVIS16.**  $\dagger$ – indicates using of additional CRF post-processing. Our method correctly segments objects in challenging conditions including strong parallax ( $1^{st}$ ,  $2^{nd}$  seq.) or small objects ( $3^{rd}$ ,  $4^{th}$ ). Notice how our method avoids segmenting the window and the shadow under the car ( $5^{th}$  seq.). In the failure case ( $6^{th}$  seq.), our method is confused by ripples and reflection in the water

Table 2: **Flow Model and Loss.** We ablate components of the flow model and loss. Each component contributes to the final performance: clipping of the flows (*Clip.*), normalization (*Norm.*), and the concentration loss (*Conc.*). Normalisation and clipping have the largest impact

| Flow Model           | Conc. | Norm. | Clip. | DAVIS16 ( $\mathcal{J}\uparrow$ ) |
|----------------------|-------|-------|-------|-----------------------------------|
| Affine (Eq. (2))     | ✓     | ✓     | ✓     | <b>71.2</b>                       |
| Constant ( $A = 0$ ) | ✓     | ✓     | ✓     | 67.7                              |
| Affine (Eq. (2))     | ✓     | ✓     |       | 68.2                              |
| Affine (Eq. (2))     | ✓     |       |       | 66.0                              |
| Affine (Eq. (2))     |       | ✓     | ✓     | 69.0                              |

## 4.2 Unsupervised Video Segmentation

Table 1 shows our model performance on the DAVIS16, STv2, and FBMS59 datasets compared against other unsupervised video segmentation approaches. We use RAFT [67] to compute optical flow, as this was adopted by previous methods. Our method achieves state-of-the-art (SoTA) performance even without considering extra post-processing steps. We exceed results of previous methods by as much as 1.4%, 1.8%, and 5.7% on DAVIS16, STv2, and FBMS59, respectively. Additionally, CRF post-processing further improves results. Fig. 2 and Fig. 3 provide a qualitative overview of our results compared with other methods. Our model provides better segmentation with sharper boundaries than other works despite complex non-rigid motion, parallax effects or lack-of-motion by only using appearance during testing. However, on challenging scenarios, our method still struggles to segment small isolated details or unconnected independent objects, as the compactness loss (5) discourages forming such masks during training.

## 4.3 Ablation Studies

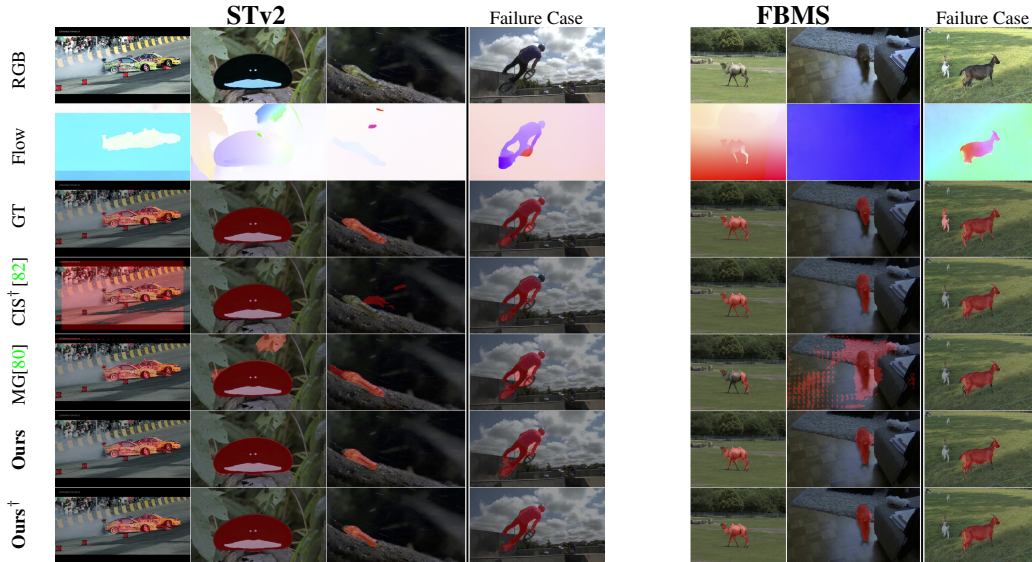


Figure 3: **Qualitative Comparison on SegTrackv2 and FBMS.** On (*STv2*), our method correctly segments objects even when motion is present in the background ( $2^{nd}$ ,  $3^{rd}$  seq.) or when appearance does not stand out from the background ( $3^{rd}$ ). However, in the failure case ( $4^{th}$ ), our method, despite producing sharp boundaries around the rider, misses the front wheel. Similarly, on (*FBMS*), our method works in presence of non-rigid motion or no motion at all ( $1^{st}$ ,  $2^{nd}$  seq.). On ( $3^{rd}$ ), we still miss additional small objects due to concentration assumptions.  $\dagger$ – indicates use of CRF post-processing.

Table 3: **Effect of Pretraining.** Our method with MaskFormer benefits from pretraining, with slight improvement offered by supervised (*CLS*) over unsupervised (*SSL*) pretraining (results use the SWIN transformer, RAFT, and the affine flow model)

| Backbone<br>pretraining | Sup.         | DAVIS16<br>$\mathcal{J}\uparrow$ | STv2<br>$\mathcal{J}\uparrow$ | FBMS59<br>$\mathcal{J}\uparrow$ |
|-------------------------|--------------|----------------------------------|-------------------------------|---------------------------------|
| None                    | $\times$     | 69.9                             | 66.6                          | 63.7                            |
| ImageNet SSL            | $\times$     | 71.2                             | 69.0                          | 66.9                            |
| ImageNet CLS            | $\checkmark$ | 71.6                             | 69.6                          | 70.6                            |

**Loss and Normalisation.** Using DAVIS16, we now study the effectiveness of the individual components by ablating aspects of the loss and flow pre-processing (Table 2). Normalisation and clipping of the flow magnitude provide significant performance improvements by reducing the effect of outliers in our approximate affine flow motion model. Furthermore, normalisation contributes by centering the distribution of residual errors across the dataset. The latter also helps by stabilizing the range of optical flow values that can vary substantially across different images and videos, much more than RGB values, and which, if unchecked, can make training less stable.

**Pretraining.** Compared to recent methods for video segmentation [53, 80], one of the benefits of our formulation is that we can leverage unsupervised pretraining for the segmentation network (Swin backbone of the MarkFormer). This enables our method to be trained in mere 5k iterations. We investigate the effect of other pretraining strategies on the performance, showing results in Table 3. Switching to a model pretrained on ImageNet with image-level supervision (*i.e.* a classification task) slightly improves performance. We attribute this to the variety of categories in the ImageNet benchmark featuring detachable objects, which might provide a more suitable representation for our network.



Table 4: **Choice of Optical Flow Method.** Measuring the influence of the method to extract optical flow. Results with self-supervised SWIN transformer backbone

| Opt. Flow   | Sup.         | DAVIS16 ( $\mathcal{J}\uparrow$ ) |
|-------------|--------------|-----------------------------------|
| [46] ARFlow | $\times$     | 64.3                              |
| [67] RAFT   | $\checkmark$ | 71.2                              |
| [65] PWCNet | $\checkmark$ | 71.6                              |

Table 5: **Fully Unsupervised Video Object Segmentation.** Comparison to the state of the art in unsupervised VOS without reliance on *any* supervision

| Method      | DAVIS16 ( $\mathcal{J}\uparrow$ ) |
|-------------|-----------------------------------|
| [80] MG     | 53.2                              |
| [47] AMD    | 57.8                              |
| <b>Ours</b> | <b>64.3</b>                       |

Table 6: **Unsupervised object segmentation benchmark CUB and three saliency detection benchmarks: DUTS, ECSSD, and DUT-OMRON (OMRON)**

|                            | CUB         |                       | DUTS        |                       | ECSSD       |                       | OMRON       |                       |
|----------------------------|-------------|-----------------------|-------------|-----------------------|-------------|-----------------------|-------------|-----------------------|
|                            | Acc         | $\mathcal{J}\uparrow$ | Acc         | $\mathcal{J}\uparrow$ | Acc         | $\mathcal{J}\uparrow$ | Acc         | $\mathcal{J}\uparrow$ |
| [28] IIC-seg               | –           | 36.5                  | –           | –                     | –           | –                     | –           | –                     |
| [6] PertGAN                | –           | 38.0                  | –           | –                     | –           | –                     | –           | –                     |
| [12] ReDO                  | 84.5        | 42.6                  | –           | –                     | –           | –                     | –           | –                     |
| [34] UISB                  | –           | 44.2                  | –           | –                     | –           | –                     | –           | –                     |
| [2] OneGAN                 | –           | 55.5                  | –           | –                     | –           | –                     | –           | –                     |
| [83] DRC                   | –           | 56.4                  | –           | –                     | –           | –                     | –           | –                     |
| [25] GANSeg                | –           | 62.9                  | –           | –                     | –           | –                     | –           | –                     |
| [72] Voynov <i>et al.</i>  | 94.0        | 71.0                  | 88.2        | 51.1                  | 90.6        | 68.4                  | 86.0        | 46.4                  |
| [52] Kyriazi <i>et al.</i> | 92.1        | 66.4                  | 89.3        | 52.8                  | <b>91.5</b> | <b>71.3</b>           | 88.3        | <b>50.9</b>           |
| <b>Ours (ARFlow)</b>       | 93.4        | 75.5                  | 92.7        | 59.7                  | 90.4        | 65.7                  | 89.9        | 46.0                  |
| <b>Ours (RAFT)</b>         | <b>95.9</b> | <b>77.5</b>           | <b>93.4</b> | <b>63.0</b>           | 90.8        | 66.8                  | <b>90.2</b> | 47.4                  |

Similarly, we consider our method without any pre-training. We train the model using same settings for 20k iterations from scratch. This results in competitive performance, matching or exceeding performance of previous methods.

**Segmentation Model.** Our method is not restricted to a specific segmentation network. We investigate whether the choice of an expressive Transformer-based architecture significantly contributes to the performance. To that end, MaskFormer is replaced with a simple convolutional U-Net architecture [61], as in EM [53], and trained from scratch to allow for a fair comparison. The U-Net based model achieves comparable results on FBMS59 and STv2 and 71.2 on DAVIS (Table 1), outperforming earlier methods even without transformers.

**Flow Estimation.** Finally, our method relies on the optical flow estimated by frozen, off-the-shelf networks. So far we have been using RAFT [67], as such optical flow network was adopted in our baselines. Instead, we consider PWCNet [65] and fully-unsupervised ARFlow [46]. Unlike previous methods (e.g., [80]), which perform worse with PWCNet, our methods maintains much of its performance (Table 4). Finally, we compare our *fully* unsupervised model (which uses self-supervised pretraining and flow) to fully unsupervised state-of-the-art methods. Appearance-Motion Decomposition (AMD) [47] works end-to-end and directly extracts motion features from pairs of images with a PWCNet-like architecture, while MotionGrouping (MG) [80] and our method use ARFlow [46] for optical flow estimation. In Table 5 we show that our method achieves a significant improvement over previous approaches.

#### 4.4 Unsupervised Image Segmentation

In the section above we have evaluated the performance of our approach for video segmentation; here we assess the image segmentation performance instead on common image segmentation and saliency benchmarks: CUB, DUTS, DUT-OMRON, and ECSSD. For this experiment, we train our model on all three motion segmentation datasets (DAVIS16, FBMS59 and STv2) jointly and apply the resulting network to the segmentation benchmarks without any further finetuning. We use the fully unsupervised version of our model (self-supervised Swin backbone and ARFlow),

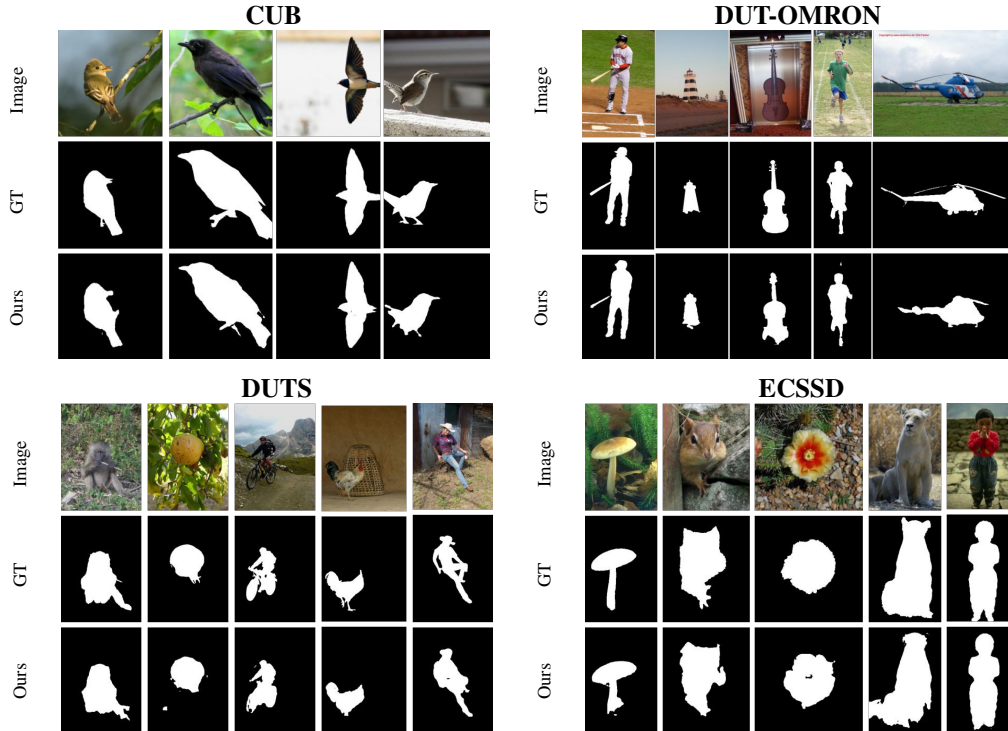


Figure 4: **Qualitative Comparison on DUT-OMRON, CUB, DUTS, ECSSD.** We train our model on a combined dataset of DAVIS16, FBMS59 and STv2. Our method can extract salient object in various environments. It works well for a wide range of classes of objects that the model is not trained with

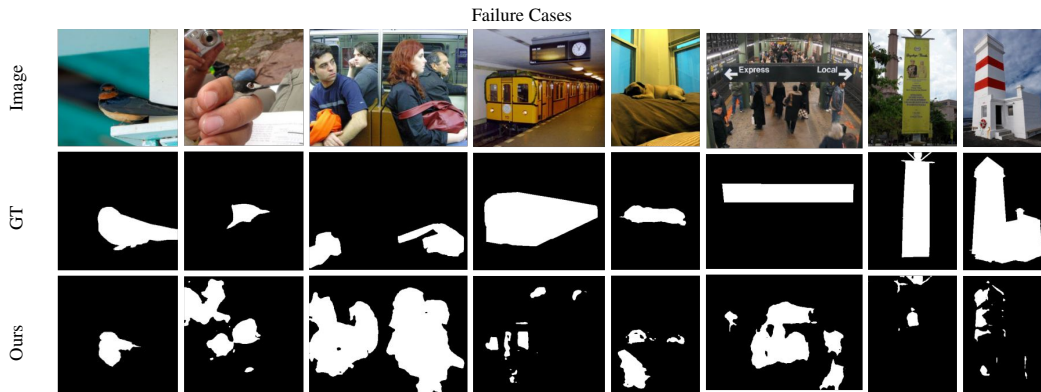


Figure 5: **Failure Cases in Object Segmentation.** They occur in ambiguous scenes (2nd and 3rd example), for objects that do not typically move (last three examples) and for images further outside the training distribution (4th and 5th example)

that learns only from unlabelled videos, to fairly compare to prior work on unsupervised image segmentation. In Table 6 we report the performance of our method, which is close to the current state-of-the-art approaches in unsupervised image segmentation on DUT-OMRON and ECSSD and outperforms then on CUB and DUTS by a significant margin (4.5% and 6.9% in IoU, respectively), demonstrating the generalization ability of our model. We also show results for our model trained with self-supervised Swin backbone and RAFT optical flow, which further improves performance. It is also worth noting that most of the prior work (except [52]) relies on dataset-specific training.

On DUTS, we also compare our approach to AMD [47], which is the only other unsupervised flow-based method that reports results on saliency detection. For a fair comparison, we evaluate the model trained on DAVIS16 and use ARFlow for unsupervised flow estimation. We adopt the metrics from [47], reporting the  $F_\beta$  score and Mean Average Error (MAE) in Table 7. Our model achieves state-of-the-art performance despite being trained on a much smaller dataset than AMD, which uses YouTube-VOS [79].

Table 7: **Comparison to AMD in saliency detection (DUTS)**

|      |             | $F_\beta$   | MAE         |
|------|-------------|-------------|-------------|
| [47] | AMD         | 60.2        | <b>0.13</b> |
|      | <b>Ours</b> | <b>63.8</b> | <b>0.13</b> |

Finally, we evaluate the model qualitatively in Fig. 4 on all four benchmarks. We observe our model works well on a diverse set of classes—humans, animals, birds, inanimate objects and even stationary structures, buildings etc., which are significantly different from the data our model was trained with. Fig. 5 shows failure cases of our model. Our model struggles with scenes where the salient objects (as annotated by humans) might seem ambiguous, e.g., in the third example annotated are the items held by the people, while our method segments all people as foreground. Another failure case occurs with salient stationary structures, e.g., in the sixth example, the model detects the people in the station rather than the banner and, in the last example, it misses the large building.

## 5 Conclusions, Limitations and Future Work

We have proposed a simple approach to exploit the synergies between motion in videos and objectness for segmenting visual objects without supervision. The key idea is using motion anticipation as a learning signal: we train an image segmentation network to predict regions that likely contain simple optical flow patterns, as these have a high chance to correspond to objects. The model can be used for video object segmentation through test-time training as the unsupervised loss informs the image model of the motion. Notably, though, since our model does not use optical flow as input, it can be also directly applied to still images. Our results show that this approach achieves state-of-the-art performance in both video and image segmentation benchmarks. We find that the complexity of the motion model is important to model complicated flow patterns that can arise even for rigid objects. Future work should thus consider extensions to more sophisticated motion patterns, accounting for the 3D shape of objects, and to separate multiple objects.

## Acknowledgements

S. C. is supported by a scholarship sponsored by Meta. L. K. is funded by EPSRC Centre for Doctoral Training in Autonomous Intelligent Machines and Systems EP/S024050/1. C. R. is supported by Innovate UK (project 71653) on behalf of UK Research and Innovation (UKRI).

## References

- [1] Daniel Bear, Chaofei Fan, Damian Mrowca, Yunzhu Li, Seth Alter, Aran Nayebi, Jeremy Schwartz, Li Fei-Fei, Jiajun Wu, Josh Tenenbaum, and Daniel L. Yamins. Learning physical graph representations from visual scenes. In Hugo Larochelle, Marc’Aurelio Ranzato, Raia Hadsell, Maria-Florina Balcan, and Hsuan-Tien Lin, editors, *Advances in Neural Information Processing Systems 33: Annual Conference on Neural Information Processing Systems 2020, NeurIPS 2020, December 6-12, 2020, virtual*, 2020.
- [2] Yaniv Benny and Lior Wolf. Onegan: Simultaneous unsupervised learning of conditional image generation, foreground segmentation, and fine-grained clustering. In *European Conference on Computer Vision*, pages 514–530. Springer, 2020.
- [3] Beril Besbinar and Pascal Frossard. Self-supervision by prediction for object discovery in videos. In *2021 IEEE International Conference on Image Processing (ICIP)*, pages 1509–1513. IEEE, 2021.
- [4] Pia Bideau and Erik Learned-Miller. It’s moving! a probabilistic model for causal motion segmentation in moving camera videos. In *European Conference on Computer Vision*, pages 433–449. Springer, 2016.
- [5] Pia Bideau, Aruni RoyChowdhury, Rakesh R Menon, and Erik Learned-Miller. The best of both worlds: Combining cnns and geometric constraints for hierarchical motion segmentation. In *Proceedings of the IEEE Conference on Computer Vision and Pattern Recognition*, pages 508–517, 2018.
- [6] Adam Bielski and Paolo Favaro. Emergence of object segmentation in perturbed generative models. *Advances in Neural Information Processing Systems*, 32, 2019.
- [7] Andrew Brock, Jeff Donahue, and Karen Simonyan. Large scale gan training for high fidelity natural image synthesis. *ArXiv*, abs/1809.11096, 2019.
- [8] Thomas Brox and Jitendra Malik. Object segmentation by long term analysis of point trajectories. In *Proceedings of the European Conference on Computer Vision (ECCV)*, 2010.
- [9] Christopher P Burgess, Loic Matthey, Nicholas Watters, Rishabh Kabra, Irina Higgins, Matt Botvinick, and Alexander Lerchner. Monet: Unsupervised scene decomposition and representation. *arXiv preprint arXiv:1901.11390*, 2019.
- [10] Sergi Caelles, Kevis-Kokitsi Maninis, Jordi Pont-Tuset, Laura Leal-Taixé, Daniel Cremers, and Luc Van Gool. One-shot video object segmentation. In *Proceedings of the IEEE conference on computer vision and pattern recognition*, pages 221–230, 2017.
- [11] Jason Chang and John W. Fisher III. Topology-constrained layered tracking with latent flow. *2013 IEEE International Conference on Computer Vision*, pages 161–168, 2013.
- [12] Mickaël Chen, Thierry Artières, and Ludovic Denoyer. Unsupervised object segmentation by redrawing. *Advances in neural information processing systems*, 32, 2019.
- [13] Bowen Cheng, Alexander G. Schwing, and Alexander Kirillov. Per-pixel classification is not all you need for semantic segmentation. In *Advances in Neural Information Processing Systems*, 2021.
- [14] Ming-Ming Cheng, Niloy J. Mitra, Xiaolei Huang, Philip H. S. Torr, and Shi-Min Hu. Global contrast based salient region detection. *IEEE Transactions on Pattern Analysis and Machine Intelligence*, 37(3): 569–582, 2015.
- [15] Eric Crawford and Joelle Pineau. Spatially invariant unsupervised object detection with convolutional neural networks. In *The Thirty-Third AAAI Conference on Artificial Intelligence*, pages 3412–3420. AAAI Press, 2019.
- [16] Eric Crawford and Joelle Pineau. Exploiting spatial invariance for scalable unsupervised object tracking. In *Thirty-Fourth AAAI Conference on Artificial Intelligence*, 2020.
- [17] A. Dosovitskiy, P. Fischer, E. Ilg, P. Häusser, C. Hazırbaş, V. Golkov, P. v.d. Smagt, D. Cremers, and T. Brox. FlowNet: Learning optical flow with convolutional networks. In *IEEE International Conference on Computer Vision (ICCV)*, 2015.
- [18] Patrick Emami, Pan He, Sanjay Ranka, and Anand Rangarajan. Efficient iterative amortized inference for learning symmetric and disentangled multi-object representations. In Marina Meila and Tong Zhang, editors, *Proceedings of the 38th International Conference on Machine Learning*, volume 139 of *Proceedings of Machine Learning Research*, pages 2970–2981. PMLR, 18–24 Jul 2021.
- [19] Martin Engelcke, Oiwi Parker Jones, and Ingmar Posner. Reconstruction bottlenecks in object-centric generative models. *arXiv preprint arXiv:2007.06245*, 2020.
- [20] Martin Engelcke, Adam R. Kosiorek, Oiwi Parker Jones, and Ingmar Posner. GENESIS: generative scene inference and sampling with object-centric latent representations. In *International Conference on Learning Representations*. OpenReview.net, 2020.
- [21] Martin Engelcke, Oiwi Parker Jones, and Ingmar Posner. Genesis-v2: Inferring unordered object representations without iterative refinement. *Advances in Neural Information Processing Systems*, 34, 2021.



- [22] Alon Faktor and Michal Irani. Video segmentation by non-local consensus voting. In *Proceedings of the British Machine Vision Conference*. BMVA Press, 2014.
- [23] Rohit Girdhar and Deva Ramanan. Cater: A diagnostic dataset for compositional actions & temporal reasoning. In *International Conference on Learning Representations*, 2020.
- [24] Klaus Greff, Raphaël Lopez Kaufman, Rishabh Kabra, Nick Watters, Christopher Burgess, Daniel Zoran, Loic Matthey, Matthew Botvinick, and Alexander Lerchner. Multi-object representation learning with iterative variational inference. In Kamalika Chaudhuri and Ruslan Salakhutdinov, editors, *Proceedings of the International Conference on Machine Learning*, volume 97 of *Proceedings of Machine Learning Research*, pages 2424–2433. PMLR, 2019.
- [25] Xingzhe He, Bastian Wandt, and Helge Rhodin. Ganseg: Learning to segment by unsupervised hierarchical image generation. *arXiv preprint arXiv:2112.01036*, 2021.
- [26] Suyog Jain, Bo Xiong, and Kristen Grauman. Fusionseg: Learning to combine motion and appearance for fully automatic segmentation of generic objects in videos. *arXiv preprint arXiv:1701.05384*, 2017.
- [27] Allan D. Jepson and Michael J. Black. Mixture models for optical flow computation. *Proceedings of IEEE Conference on Computer Vision and Pattern Recognition*, pages 760–761, 1993.
- [28] Xu Ji, Joao F Henriques, and Andrea Vedaldi. Invariant information clustering for unsupervised image classification and segmentation. In *Proceedings of the IEEE/CVF International Conference on Computer Vision*, pages 9865–9874, 2019.
- [29] Jindong Jiang and Sungjin Ahn. Generative neurosymbolic machines. *Advances in Neural Information Processing Systems*, 33:12572–12582, 2020.
- [30] Jindong Jiang\*, Sepehr Janghorbani\*, Gerard De Melo, and Sungjin Ahn. Scalor: Generative world models with scalable object representations. In *International Conference on Learning Representations*, 2020.
- [31] Justin Johnson, Bharath Hariharan, Laurens Van Der Maaten, Li Fei-Fei, C Lawrence Zitnick, and Ross Girshick. Clevr: A diagnostic dataset for compositional language and elementary visual reasoning. In *Proceedings of the IEEE conference on computer vision and pattern recognition*, pages 2901–2910, 2017.
- [32] N. Jojic and B.J. Frey. Learning flexible sprites in video layers. In *Proceedings of the 2001 IEEE Computer Society Conference on Computer Vision and Pattern Recognition. CVPR 2001*, volume 1, pages I–I, 2001.
- [33] Rishabh Kabra, Daniel Zoran, Goker Erdogan, Loic Matthey, Antonia Creswell, Matthew Botvinick, Alexander Lerchner, and Christopher P Burgess. Simone: View-invariant, temporally-abstracted object representations via unsupervised video decomposition. *arXiv preprint arXiv:2106.03849*, 2021.
- [34] Asako Kanezaki. Unsupervised image segmentation by backpropagation. In *2018 IEEE international conference on acoustics, speech and signal processing (ICASSP)*, pages 1543–1547. IEEE, 2018.
- [35] Laurynas Karazija, Iro Laina, and Christian Rupprecht. Clevrtex: A texture-rich benchmark for unsupervised multi-object segmentation. In *Thirty-fifth Conference on Neural Information Processing Systems Datasets and Benchmarks Track (Round 2)*, 2021.
- [36] Yoni Kasten, Dolev Ofri, Oliver Wang, and Tali Dekel. Layered neural atlases for consistent video editing. *arXiv.cs, abs/2109.11418*, 2021.
- [37] Margret Keuper. Higher-order minimum cost lifted multicuts for motion segmentation. *2017 IEEE International Conference on Computer Vision (ICCV)*, pages 4252–4260, 2017.
- [38] Margret Keuper, Bjoern Andres, and Thomas Brox. Motion trajectory segmentation via minimum cost multicuts. In *2015 IEEE International Conference on Computer Vision (ICCV)*, pages 3271–3279, 2015.
- [39] Margret Keuper, Siyu Tang, Bjoern Andres, Thomas Brox, and Bernt Schiele. Motion segmentation and multiple object tracking by correlation co-clustering. *IEEE Transactions on Pattern Analysis and Machine Intelligence*, 42(1):140–153, 2020.
- [40] Thomas Kipf, Gamaleldin F Elsayed, Aravindh Mahendran, Austin Stone, Sara Sabour, Georg Heigold, Rico Jonschkowski, Alexey Dosovitskiy, and Klaus Greff. Conditional object-centric learning from video. *arXiv preprint arXiv:2111.12594*, 2021.
- [41] Adam Kosior, Hyunjik Kim, Yee Whye Teh, and Ingmar Posner. Sequential attend, infer, repeat: Generative modelling of moving objects. In S. Bengio, H. Wallach, H. Larochelle, K. Grauman, N. Cesa-Bianchi, and R. Garnett, editors, *Advances in Neural Information Processing Systems*, volume 31. Curran Associates, Inc., 2018.
- [42] Hala Lamdouar, Charig Yang, Weidi Xie, and Andrew Zisserman. Betrayed by motion: Camouflaged object discovery via motion segmentation. In *Proceedings of the Asian Conference on Computer Vision (ACCV)*, November 2020.

- [43] Fuxin Li, Taeyoung Kim, Ahmad Humayun, David Tsai, and James M. Rehg. Video segmentation by tracking many figure-ground segments. *2013 IEEE International Conference on Computer Vision*, pages 2192–2199, 2013.
- [44] Siyang Li, Bryan Seybold, Alexey Vorobyov, Alireza Fathi, Qin Huang, and C-C Jay Kuo. Instance embedding transfer to unsupervised video object segmentation. In *Proceedings of the IEEE conference on computer vision and pattern recognition*, pages 6526–6535, 2018.
- [45] Zhixuan Lin, Yi-Fu Wu, Skand Vishwanath Peri, Weihao Sun, Gautam Singh, Fei Deng, Jindong Jiang, and Sungjin Ahn. SPACE: unsupervised object-oriented scene representation via spatial attention and decomposition. In *International Conference on Learning Representations*. OpenReview.net, 2020.
- [46] Liang Liu, Jiangning Zhang, Ruifei He, Yong Liu, Yabiao Wang, Ying Tai, Donghao Luo, Chengjie Wang, Jilin Li, and Feiyue Huang. Learning by analogy: Reliable supervision from transformations for unsupervised optical flow estimation. In *Proceedings of the IEEE/CVF Conference on Computer Vision and Pattern Recognition (CVPR)*, June 2020.
- [47] Runtao Liu, Zhirong Wu, Stella Yu, and Stephen Lin. The emergence of objectness: Learning zero-shot segmentation from videos. *Advances in Neural Information Processing Systems*, 34, 2021.
- [48] Ze Liu, Yutong Lin, Yue Cao, Han Hu, Yixuan Wei, Zheng Zhang, Stephen Lin, and Baining Guo. Swin transformer: Hierarchical vision transformer using shifted windows. In *Proceedings of the IEEE/CVF International Conference on Computer Vision*, pages 10012–10022, 2021.
- [49] Francesco Locatello, Dirk Weissenborn, Thomas Unterthiner, Aravindh Mahendran, Georg Heigold, Jakob Uszkoreit, Alexey Dosovitskiy, and Thomas Kipf. Object-centric learning with slot attention. *arXiv preprint arXiv:2006.15055*, 2020.
- [50] Xiankai Lu, Wenguan Wang, Chao Ma, Jianbing Shen, Ling Shao, and Fatih Porikli. See more, know more: Unsupervised video object segmentation with co-attention siamese networks. In *Proceedings of the IEEE/CVF Conference on Computer Vision and Pattern Recognition*, pages 3623–3632, 2019.
- [51] Aravindh Mahendran, James Thewlis, and Andrea Vedaldi. Self-supervised segmentation by grouping optical-flow. In *Proceedings of the European Conference on Computer Vision (ECCV) Workshops*, September 2018.
- [52] Luke Melas-Kyriazi, Christian Rupprecht, Iro Laina, and Andrea Vedaldi. Finding an unsupervised image segmenter in each of your deep generative models. In *International Conference on Learning Representations*, 2022.
- [53] Etienne Meunier, Anaïs Badoual, and Patrick Bouthemy. Em-driven unsupervised learning for efficient motion segmentation. *CoRR*, abs/2201.02074, 2022.
- [54] Ben Mildenhall, Pratul P. Srinivasan, Matthew Tancik, Jonathan T. Barron, Ravi Ramamoorthi, and Ren Ng. NeRF: Representing scenes as neural radiance fields for view synthesis. In *Proc. ECCV*, 2020.
- [55] Cheol-Hui Min, Jinseok Bae, Junho Lee, and Young Min Kim. Gatsbi: Generative agent-centric spatio-temporal object interaction. In *Proceedings of the IEEE/CVF Conference on Computer Vision and Pattern Recognition*, pages 3074–3083, 2021.
- [56] Tam Nguyen, Maximilian Dax, Chaithanya Kumar Mummadi, Nhung Ngo, Thi Hoai Phuong Nguyen, Zhongyu Lou, and Thomas Brox. Deepusps: Deep robust unsupervised saliency prediction via self-supervision. In H. Wallach, H. Larochelle, A. Beygelzimer, F. d'Alché-Buc, E. Fox, and R. Garnett, editors, *Advances in Neural Information Processing Systems*, volume 32. Curran Associates, Inc., 2019.
- [57] Peter Ochs, Jitendra Malik, and Thomas Brox. Segmentation of moving objects by long term video analysis. *IEEE Transactions on Pattern Analysis and Machine Intelligence*, 36:1187–1200, 2014.
- [58] Yassine Ouali, Celine Hudelot, and Myriam Tami. Autoregressive unsupervised image segmentation. In *Proceedings of the European Conference on Computer Vision (ECCV)*, August 2020.
- [59] Anestis Papazoglou and Vittorio Ferrari. Fast object segmentation in unconstrained video. In *Proceedings of the IEEE International Conference on Computer Vision (ICCV)*, December 2013.
- [60] F. Perazzi, J. Pont-Tuset, B. McWilliams, L. Van Gool, M. Gross, and A. Sorkine-Hornung. A benchmark dataset and evaluation methodology for video object segmentation. In *Computer Vision and Pattern Recognition*, 2016.
- [61] Olaf Ronneberger, Philipp Fischer, and Thomas Brox. U-net: Convolutional networks for biomedical image segmentation. In *International Conference on Medical image computing and computer-assisted intervention*, pages 234–241. Springer, 2015.
- [62] Olga Russakovsky, Jia Deng, Hao Su, Jonathan Krause, Sanjeev Satheesh, Sean Ma, Zhiheng Huang, Andrej Karpathy, Aditya Khosla, Michael Bernstein, et al. Imagenet large scale visual recognition challenge. *International journal of computer vision*, 115(3):211–252, 2015.

- [63] Jianping Shi, Qiong Yan, Li Xu, and Jiaya Jia. Hierarchical image saliency detection on extended cssd. *IEEE Transactions on Pattern Analysis and Machine Intelligence*, 38(4):717–729, 2016.
- [64] Elizabeth S Spelke. Principles of object perception. *Cognitive science*, 14(1):29–56, 1990.
- [65] Deqing Sun, Xiaodong Yang, Ming-Yu Liu, and Jan Kautz. Pwc-net: Cnns for optical flow using pyramid, warping, and cost volume. In *Proceedings of the IEEE Conference on Computer Vision and Pattern Recognition (CVPR)*, June 2018.
- [66] Narayanan Sundaram, Thomas Brox, and Kurt Keutzer. Dense point trajectories by GPU-Accelerated large displacement optical flow. In *Proceedings of the European Conference on Computer Vision (ECCV)*, 2010.
- [67] Zachary Teed and Jia Deng. Raft: Recurrent all-pairs field transforms for optical flow. In *European Conference on Computer Vision (ECCV)*, 2020.
- [68] Pavel Tokmakov, Cordelia Schmid, and Karteek Alahari. Learning to segment moving objects. *Int. J. Comput. Vision*, 127(3):282–301, mar 2019. ISSN 0920-5691.
- [69] Philip H. S. Torr. Geometric motion segmentation and model selection. *Philosophical Transactions of the Royal Society of London. Series A: Mathematical, Physical and Engineering Sciences*, 356:1321 – 1340, 1998.
- [70] Yi-Hsuan Tsai, Ming-Hsuan Yang, and Michael J. Black. Video segmentation via object flow. In *2016 IEEE Conference on Computer Vision and Pattern Recognition (CVPR)*, pages 3899–3908, 2016.
- [71] Dmitry Ulyanov, Andrea Vedaldi, and Victor S. Lempitsky. Deep image prior. *IJCV*, 128(7):1867–1888, 2020.
- [72] Andrey Voynov, Stanislav Morozov, and Artem Babenko. Object segmentation without labels with large-scale generative models. In *International Conference on Machine Learning*, pages 10596–10606. PMLR, 2021.
- [73] Johan Wagemans, Jacob Feldman, Sergei Gepshtein, Ruth Kimchi, James R Pomerantz, Peter A Van der Helm, and Cees Van Leeuwen. A century of gestalt psychology in visual perception: Ii. conceptual and theoretical foundations. *Psychological bulletin*, 138(6):1218, 2012.
- [74] Lijun Wang, Huchuan Lu, Yifan Wang, Mengyang Feng, Dong Wang, Baocai Yin, and Xiang Ruan. Learning to detect salient objects with image-level supervision. In *The IEEE Conference on Computer Vision and Pattern Recognition (CVPR)*, 2017.
- [75] Wenguan Wang, Jianbing Shen, Ruigang Yang, and Fatih Porikli. Saliency-aware video object segmentation. *IEEE Transactions on Pattern Analysis and Machine Intelligence*, 40(1):20–33, 2018.
- [76] Yichen Wei, Fang Wen, Wangjiang Zhu, and Jian Sun. Geodesic saliency using background priors. In *ECCV*, 2012.
- [77] P. Welinder, S. Branson, T. Mita, C. Wah, F. Schroff, S. Belongie, and P. Perona. Caltech-UCSD Birds 200. Technical Report CNS-TR-2010-001, California Institute of Technology, 2010.
- [78] Zhenda Xie, Yutong Lin, Zhuliang Yao, Zheng Zhang, Qi Dai, Yue Cao, and Han Hu. Self-supervised learning with swin transformers. *arXiv preprint arXiv:2105.04553*, 2021.
- [79] Ning Xu, Linjie Yang, Yuchen Fan, Dingcheng Yue, Yuchen Liang, Jianchao Yang, and Thomas Huang. Youtube-vos: A large-scale video object segmentation benchmark. *arXiv preprint arXiv:1809.03327*, 2018.
- [80] Charig Yang, Hala Lamdouar, Erika Lu, Andrew Zisserman, and Weidi Xie. Self-supervised video object segmentation by motion grouping. In *Proceedings of the IEEE/CVF International Conference on Computer Vision*, pages 7177–7188, 2021.
- [81] Chuan Yang, Lihe Zhang, Huchuan Lu, Xiang Ruan, and Ming-Hsuan Yang. Saliency detection via graph-based manifold ranking. In *Computer Vision and Pattern Recognition (CVPR), 2013 IEEE Conference on*, pages 3166–3173. IEEE, 2013.
- [82] Yanchao Yang, Antonio Loquercio, Davide Scaramuzza, and Stefano Soatto. Unsupervised moving object detection via contextual information separation. In *Proceedings of the IEEE/CVF Conference on Computer Vision and Pattern Recognition (CVPR)*, June 2019.
- [83] Peiyu Yu, Sirui Xie, Xiaojian Ma, Yixin Zhu, Ying Nian Wu, and Song-Chun Zhu. Unsupervised foreground extraction via deep region competition. *Advances in Neural Information Processing Systems*, 34, 2021.
- [84] Polina Zablotkskaia, Edoardo A Dominici, Leonid Sigal, and Andreas M Lehmann. Unsupervised video decomposition using spatio-temporal iterative inference. *arXiv preprint arXiv:2006.14727*, 2020.
- [85] Yu Zeng, Yunzhi Zhuge, Huchuan Lu, Lihe Zhang, Mingyang Qian, and Yizhou Yu. Multi-source weak supervision for saliency detection. In *IEEE Conference on Computer Vision and Pattern Recognition*, 2019.

- [86] Jing Zhang, T. Zhang, Yuchao Dai, Mehrtash Harandi, and Richard I. Hartley. Deep unsupervised saliency detection: A multiple noisy labeling perspective. *2018 IEEE/CVF Conference on Computer Vision and Pattern Recognition*, pages 9029–9038, 2018.



## Supplementary Material

In this supplementary material, we provide further details on our training parameters in Appendix A. We provide the closed form solution of the fitting of the flow model  $\theta$  in Appendix B. Appendix C demonstrates how we can compute compactness in  $O(|\Omega|)$ , instead of the main paper’s  $O(|\Omega|^2)$  formulation. More qualitative results are presented in Appendix D.

### A Training Hyperparameters

We further detail the hyperparameters used during the training of MaskFormer<sup>3</sup>. In addition to using learning rate of  $1.5 \times 10^{-4}$ , a schedule of linear warm-up from  $1.0 \times 10^{-6}$  to  $1.5 \times 10^{-4}$  over 1.5k iteration and polynomial decay afterwards was deployed. We gradually unfreeze the pre-trained Swin backbone. All Transformer layers are initially frozen with the last 2 unfreezing at 500 iterations and the rest at 1000. We do not train the patch embedding projection layers.

For experiments using U-Net<sup>4</sup>, we use the standard 4-layer version. The batch-size is increased to 16 and learning rate to  $7.0 \times 10^{-4}$ . We also clip the gradients only when 2-norm exceeds 5.0. All other settings, including optimizer and learning rate schedules, are kept the same. U-Net is not pre-trained and thus is trained from scratch.

### B Closed Form Solution for Loss using Affine Flow Model

Consider one of the two regions  $m \in \{0, 1\}$  and define  $w_u \propto P(m_u = m | I, \Phi)$  the posterior probability for that region, normalized so that  $\sum_{u \in \Omega} w_u = 1$  (the scaling factor does not matter for the purpose of finding the minimizer). We can obtain the minimizer  $(A^*, b^*)$  and minimum of the energy

$$E(A, b) = \sum_{u \in \Omega} w_u \|F_u - Au - b\|^2 \quad (8)$$

as follows. Define

$$\bar{u} = \begin{bmatrix} u \\ 1 \end{bmatrix}, \quad M = \begin{bmatrix} A & b \end{bmatrix} \in \mathbb{R}^{2 \times 3}$$

so that the energy can be rewritten more compactly as

$$E(M) = \sum_{u \in \Omega} w_u \|F_u - M\bar{u}\|^2 = \text{tr} (\Lambda_{FF} - M\Lambda_{\Omega F} - \Lambda_{F\Omega}M^\top + M\Lambda_{\Omega\Omega}M^\top)$$

where

$$\Lambda_{FF} = \sum_{u \in \Omega} w_u F_u F_u^\top, \quad \Lambda_{F\Omega} = \sum_{u \in \Omega} w_u F_u \bar{u}^\top, \quad \Lambda_{\Omega F} = \Lambda_{F\Omega}^\top, \quad \Lambda_{\Omega\Omega} = \sum_{u \in \Omega} w_u \bar{u} \bar{u}^\top.$$

are the (uncentered) second moment matrices of the flow  $F_u$  and homogeneous coordinate vectors  $\bar{u}$ . By inspection of the trace term, the gradient of the energy is given by:

$$\frac{dE(M)}{dM} = 2 (\Lambda_{F\Omega} - M\Lambda_{\Omega\Omega})$$

Hence, the optimal regression matrix  $M^*$  and corresponding energy value are

$$M^* = \Lambda_{F\Omega} \Lambda_{\Omega\Omega}^{-1}, \quad E(M^*) = \text{tr} (\Lambda_{FF} - M^* \Lambda_{\Omega\Omega}).$$

Somewhat more intuitive results can be obtained by centering the moments and resolving for  $A$  and  $b$  instead of  $M$ . Specifically, define:

$$\mu_\Omega = \sum_{u \in \Omega} w_u u, \quad \mu_F = \sum_{u \in \Omega} w_u F_u.$$

<sup>3</sup>Implementation from <https://github.com/facebookresearch/MaskFormer>.

<sup>4</sup>Implementation from <https://github.com/milesial/Pytorch-UNet>.

The covariance matrices of the vectors are:

$$\begin{aligned}\Sigma_{FF} &= \sum_{u \in \Omega} w_u (F_u - \mu_F)(F_u - \mu_F)^\top, \quad \Sigma_{F\Omega} = \sum_{u \in \Omega} w_u (F_u - \mu_F)(u - \mu_\Omega)^\top, \\ \Sigma_{\Omega F} &= \Lambda_{F\Omega}^\top, \quad \Sigma_{\Omega\Omega} = \sum_{u \in \Omega} w_u (u - \mu_\Omega)(u - \mu_\Omega)^\top.\end{aligned}$$

It is easy to check that

$$\begin{aligned}\Lambda_{FF} &= \Sigma_{FF} + \mu_F \mu_F^\top, \quad \Lambda_{F\bar{\Omega}} = [\Sigma_{F\Omega} + \mu_F \mu_\Omega^\top \quad \mu_F], \\ \Lambda_{\bar{\Omega}\bar{\Omega}} &= \begin{bmatrix} \Sigma_{\Omega\Omega} + \mu_\Omega \mu_\Omega^\top & \mu_\Omega \\ \mu_\Omega^\top & 1 \end{bmatrix}.\end{aligned}$$

From this:

$$\begin{aligned}M^* &= \Lambda_{F\bar{\Omega}} \Lambda_{\bar{\Omega}\bar{\Omega}}^{-1} = [\Sigma_{F\Omega} + \mu_F \mu_\Omega^\top \quad \mu_F] \begin{bmatrix} \Sigma_{\Omega\Omega} + \mu_\Omega \mu_\Omega^\top & \mu_\Omega \\ \mu_\Omega^\top & 1 \end{bmatrix}^{-1} \\ &= [\Sigma_{F\Omega} + \mu_F \mu_\Omega^\top \quad \mu_F] \begin{bmatrix} \Sigma_{\Omega\Omega}^{-1} & -\Sigma_{\Omega\Omega}^{-1} \mu_\Omega \\ -\mu_\Omega^\top \Sigma_{\Omega\Omega}^{-1} & 1 + \mu_\Omega^\top \Sigma_{\Omega\Omega}^{-1} \mu_\Omega \end{bmatrix} \\ &= [\Sigma_{F\Omega} \Sigma_{\Omega\Omega}^{-1} \quad \mu_F - \Sigma_{F\Omega} \Sigma_{\Omega\Omega}^{-1} \mu_\Omega] = [A^* \quad b^*].\end{aligned}$$

Hence, the optimal regression coefficients and energy value are also given by:

$$A^* = \Sigma_{F\Omega} \Sigma_{\Omega\Omega}^{-1}, \quad b^* = \mu_F - A^* \mu_\Omega, \quad E(A^*, b^*) = \text{tr}(\Sigma_{FF} - A^* \Sigma_{\Omega F} - b^* \mu_F^\top).$$

## C Compactness Loss

We measure compactness as the average squared  $L^2$  distance between pixels in the foreground region. We define  $\mu = \sum_{u \in \Omega} u \cdot P(m_u = 1 | \Phi, I)$ , where  $P(m_i = 1 | \Phi, I)$  is the *spatial* probability distribution function for the foreground mask implying  $\sum_{u \in \Omega} P(m_u = 1 | \Phi, I) = 1$ .

$$\begin{aligned}\mathcal{L}_{\text{cmp}}(\Phi, I) &= \sum_{u, v \in \Omega} \|u - v\|^2 \cdot w_u w_v, \text{ where } w_j = P(m_j = 1 | \Phi, I) \\ &= \sum_{u, v \in \Omega} w_u w_v (\|u - \mu\|^2 + \langle u - \mu, \mu - v \rangle + \langle \mu - v, u - \mu \rangle + \|\mu - v\|^2) \\ &= \sum_{u, v \in \Omega} w_u w_v (2\|u - \mu\|^2 + 2\langle u - \mu, \mu - v \rangle) \\ &= 2 \sum_{u, v \in \Omega} w_u w_v \|u - \mu\|^2 + 2 \sum_{u, v \in \Omega} w_u w_v (\mu(u - \mu) - v(u - \mu)) \\ &= 2 \sum_{v \in \Omega} w_v \sum_{u \in \Omega} w_u \|u - \mu\|^2 + 2\mu \sum_{v \in \Omega} w_v \sum_{u \in \Omega} w_u (u - \mu) - 2 \sum_{v \in \Omega} w_v v \sum_{u \in \Omega} w_u (u - \mu) \\ &= 2 \sum_{u \in \Omega} w_u \|u - \mu\|^2 + 2\mu \sum_{u \in \Omega} w_u (u - \mu) - 2\mu \sum_{u \in \Omega} w_u (u - \mu) \\ &= 2 \sum_{u \in \Omega} \|u - \mu\|^2 \cdot P(m_u = 1 | \Phi, I) \\ &\propto \sum_{u \in \Omega} \|u - \mu\|^2 \cdot P(m_u = 1 | \Phi, I)\end{aligned}$$

## D Additional Listing of Results

Here, we provide a further breakdown of our results. Table 8, Table 9, and Table 10 show per sequence evaluation results on the video segmentation mode. Videos of the outputs accompany this supplemental material.

Table 8: Result breakdown on DAVIS16 validation sequences. ( $M$ ), ( $R$ ), and ( $D$ ) are mean, recall and decay of IoU, respectively

| Sequence           | <i>w/o CRF</i>   |                  |                  | <i>w/ CRF</i>    |                  |                  |
|--------------------|------------------|------------------|------------------|------------------|------------------|------------------|
|                    | $\mathcal{J}(M)$ | $\mathcal{J}(R)$ | $\mathcal{J}(D)$ | $\mathcal{J}(M)$ | $\mathcal{J}(R)$ | $\mathcal{J}(D)$ |
| blackswan          | 48.1             | 60.4             | -13.8            | 49.7             | 64.6             | -16.3            |
| bmx-trees          | 49.7             | 59.0             | 10.6             | 50.8             | 61.5             | 9.5              |
| breakdance         | 68.2             | 98.8             | 5.6              | 69.4             | 98.8             | 4.8              |
| camel              | 74.4             | 100.0            | 13.5             | 75.9             | 100.0            | 13.5             |
| car-roundabout     | 87.0             | 100.0            | 3.8              | 87.5             | 100.0            | 2.8              |
| car-shadow         | 87.3             | 100.0            | 1.6              | 86.1             | 100.0            | 2.2              |
| cows               | 83.1             | 100.0            | 4.3              | 84.2             | 100.0            | 4.2              |
| dance-twirl        | 72.7             | 100.0            | -7.9             | 74.0             | 98.9             | -7.0             |
| dog                | 78.0             | 100.0            | -0.1             | 80.0             | 100.0            | -0.2             |
| drift-chicane      | 78.9             | 100.0            | -10.1            | 80.0             | 100.0            | -16.0            |
| drift-straight     | 75.4             | 100.0            | 7.0              | 76.1             | 100.0            | 7.2              |
| goat               | 53.0             | 67.0             | 18.5             | 56.3             | 76.1             | 20.5             |
| horsejump-high     | 78.9             | 100.0            | 8.4              | 84.2             | 100.0            | 6.2              |
| kite-surf          | 45.3             | 58.3             | 40.3             | 50.5             | 70.8             | 43.6             |
| libby              | 72.4             | 100.0            | 10.9             | 77.2             | 100.0            | 9.8              |
| motocross-jump     | 72.7             | 94.7             | -0.9             | 74.3             | 94.7             | -0.5             |
| paragliding-launch | 57.8             | 61.5             | 30.3             | 60.2             | 62.8             | 32.3             |
| parkour            | 82.9             | 100.0            | -2.8             | 87.6             | 100.0            | -0.1             |
| scooter-black      | 80.4             | 100.0            | -0.6             | 81.3             | 100.0            | -1.6             |
| soapbox            | 82.6             | 100.0            | 1.5              | 85.6             | 100.0            | 2.6              |
| Average            | 71.4             | 90.0             | 6.0              | 73.5             | 91.4             | 5.9              |

For unsupervised object detection, we show some additional qualitative results for CUB in Fig. 6, DUT-OMRON in Fig. 7, DUTS in Fig. 8, and ECSSD in Fig. 9. Our model, trained on a combined dataset of DAVIS16, FBMS59 and STv2, is robust enough to handle a wide array of classes from the above datasets in varying context. Our model can segment both stationary and non-stationary objects and works well when multiple objects are in the foreground. In Fig. 10, we show a few failure cases for all datasets, where the model struggles mostly with ambiguous foreground objects and, in particular, with close-ups of stationary objects, e.g., signs (ECSSD) and buildings (DUT-OMRON). The model also has issues with boundaries for many objects, *i.e.* the foreground objects are correctly identified but the model fails to fully segment them. For example, in DUTS, the snake in the first image has a well segmented head, however, the model does not segment its body accurately.

Table 9: Sequence breakdown on SegTrackv2 dataset

| Sequence         | <i>w/o CRF</i><br>$\mathcal{J}(M)$ | <i>w/ CRF</i><br>$\mathcal{J}(M)$ |
|------------------|------------------------------------|-----------------------------------|
| drift            | 82.1                               | 81.7                              |
| birdfall         | 1.6                                | 1.7                               |
| girl             | 76.1                               | 78.2                              |
| cheetah          | 36.7                               | 31.5                              |
| worm             | 77.4                               | 81.2                              |
| parachute        | 89.4                               | 92.9                              |
| monkeydog        | 26.7                               | 27.8                              |
| hummingbird      | 51.9                               | 52.2                              |
| soldier          | 70.9                               | 70.6                              |
| bmh              | 58.6                               | 59.8                              |
| frog             | 76.1                               | 83.0                              |
| penguin          | 50.8                               | 51.1                              |
| monkey           | 73.0                               | 76.4                              |
| bird of paradise | 90.4                               | 93.2                              |
| Seq. Avg.        | 61.6                               | 62.9                              |
| Frame Avg.       | 69.9                               | 73.1                              |

Table 10: Sequence breakdown on FBMS59 dataset

| Sequence   | <i>w/o CRF</i><br>$\mathcal{J}(M)$ | <i>w/ CRF</i><br>$\mathcal{J}(M)$ |
|------------|------------------------------------|-----------------------------------|
| camel01    | 77.1                               | 84.5                              |
| cars1      | 80.8                               | 80.1                              |
| cars10     | 30.1                               | 29.4                              |
| cars4      | 80.2                               | 81.8                              |
| cars5      | 48.7                               | 49.3                              |
| cats01     | 77.9                               | 83.3                              |
| cats03     | 60.0                               | 59.5                              |
| cats06     | 50.8                               | 56.9                              |
| dogs01     | 72.1                               | 73.0                              |
| dogs02     | 79.0                               | 81.0                              |
| farm01     | 83.4                               | 83.8                              |
| giraffes01 | 60.9                               | 63.8                              |
| goats01    | 63.7                               | 66.4                              |
| horses02   | 75.0                               | 79.3                              |
| horses04   | 75.6                               | 80.4                              |
| horses05   | 60.5                               | 62.7                              |
| lion01     | 68.4                               | 69.6                              |
| marple12   | 74.9                               | 73.7                              |
| marple2    | 75.7                               | 77.4                              |
| marple4    | 82.0                               | 84.9                              |
| marple6    | 79.2                               | 79.9                              |
| marple7    | 69.6                               | 70.3                              |
| marple9    | 47.0                               | 47.0                              |
| people03   | 75.3                               | 76.7                              |
| people1    | 74.7                               | 79.5                              |
| people2    | 75.0                               | 76.6                              |
| rabbits02  | 80.4                               | 80.8                              |
| rabbits03  | 45.6                               | 47.1                              |
| rabbits04  | 14.2                               | 14.9                              |
| tennis     | 64.7                               | 65.8                              |
| Seq. Avg.  | 66.8                               | 68.6                              |
| Frame Avg. | 67.2                               | 69.4                              |



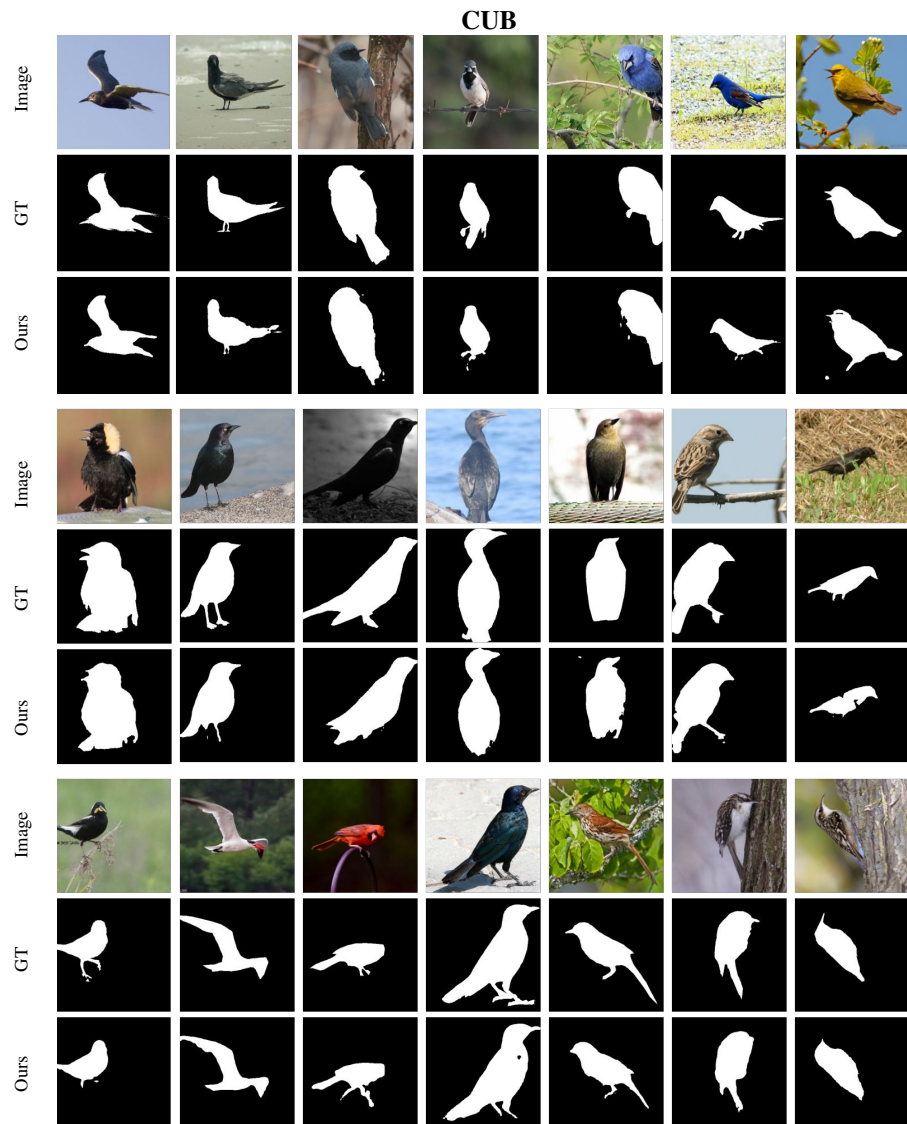


Figure 6: **Qualitative Comparison on CUB.** We train our model on a combined dataset of DAVIS16, FBMS59 and STv2. Our method can extract birds in different environments and poses. Our model can segment different species of birds

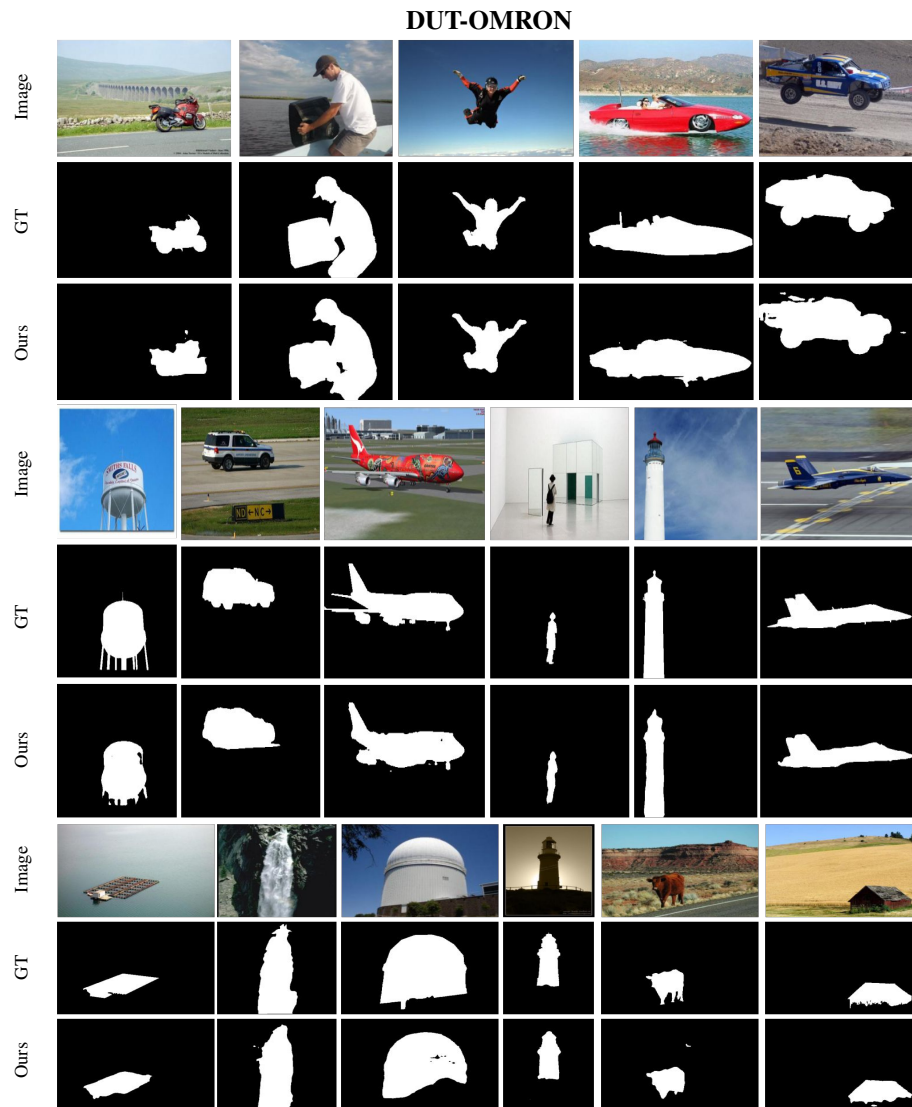


Figure 7: **Qualitative Comparison on DUT-OMRON.** We train our model on a combined dataset of DAVIS16, FBMS59 and STv2. Our model can segment both stationary and non-stationary objects and is robust enough to work on a wide range of classes

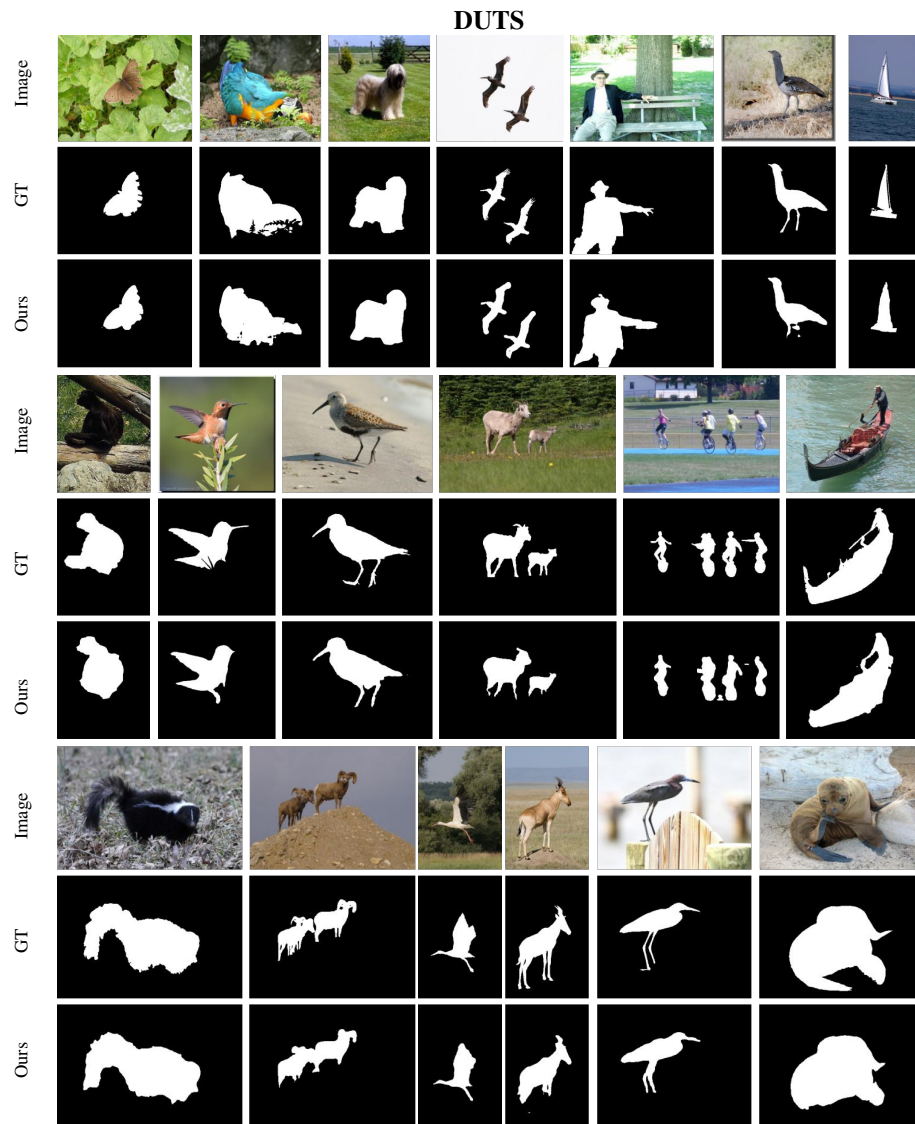


Figure 8: **Qualitative Comparison on DUTS.** We train our model on a combined dataset of DAVIS16, FBMS59 and STv2. We can segment a wide array of classes. Our model performs well on scenes where multiple objects are in the foreground

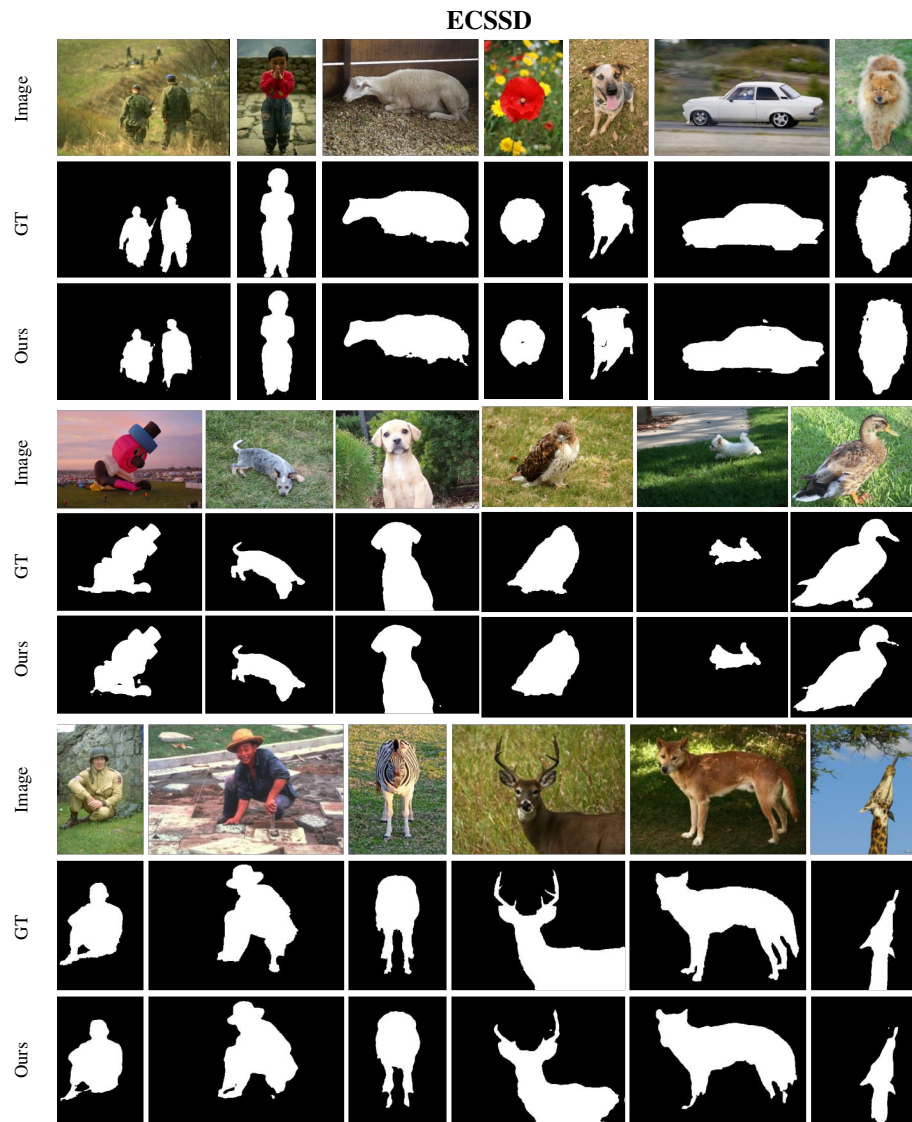


Figure 9: **Qualitative Comparison on ECSSD.** We train our model on a combined dataset of DAVIS16, FBMS59 and STv2. Our model can segment objects from different classes in complex poses

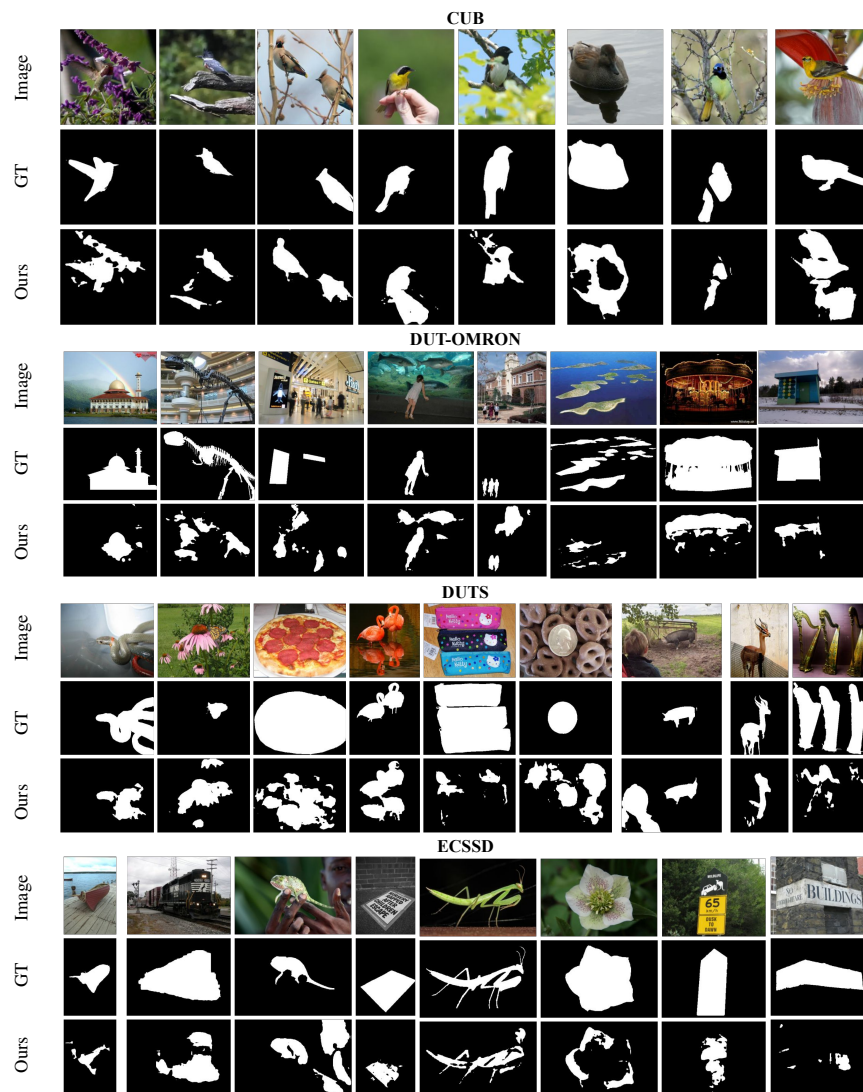


Figure 10: **Qualitative Comparison of Failure Cases.** We train our model on a combined dataset of DAVIS16, FBMS59 and STv2. Our method can extract salient object in various environments. The model has difficulty where the foreground object is ambiguous — when there are multiple prominent objects but only few are annotated as salient object. The model also has issues with predicting the object boundaries well for some instances